

## Tracing ions in the cusp and low-latitude boundary layer using multispacecraft observations and a global MHD simulation

S. A. Fuselier,<sup>1</sup> J. Berchem,<sup>2</sup> K. J. Trattner,<sup>1</sup> and R. Friedel<sup>3</sup>

Received 9 May 2001; revised 3 October 2001; accepted 3 October 2001; published 6 September 2002.

[1] High-latitude observations from the Polar spacecraft on 21 January 1998 show a region of closed magnetic field lines containing several distinct solar wind ion populations in the energy range from  $<10$  eV to  $>200$  keV  $e^{-1}$ . Precipitating ion fluxes in this region are consistent with the low-latitude boundary layer (LLBL). A global MHD simulation of this event (using input from the Wind spacecraft upstream from the Earth's bow shock) reproduces Geotail and Interball/Tail spacecraft observations in the outer magnetosphere and magnetosheath. These results demonstrate that the simulation faithfully reproduces the global magnetic field configuration of the magnetosheath and magnetosphere and provides confidence for the interpretation of the LLBL observations from Polar. Results from the simulation show that a single evolutionary process of plasma entry into the cusp and evolution to the LLBL can account for the development of a multi-energy ion population of solar wind origin on closed magnetic field lines in the magnetosphere. Sources with direct access to the ultimately closed LLBL field lines observed by Polar are the dayside magnetosheath (low-energy ions below 3 keV  $e^{-1}$ ), the quasi-parallel bow shock (higher-energy ions between 3 and 100 keV  $e^{-1}$ ), and possibly the duskside magnetopause (highest-energy ions above 100 keV  $e^{-1}$ ). *INDEX TERMS:* 2724 Magnetospheric Physics: Magnetopause, cusp, and boundary layers; 2753 Magnetospheric Physics: Numerical modeling; 7835 Space Plasma Physics: Magnetic reconnection; 2154 Interplanetary Physics: Planetary bow shocks; *KEYWORDS:* magnetic reconnection, particle precipitation, charged particle motion

**Citation:** Fuselier, S. A., J. Berchem, K. J. Trattner, and R. Friedel, Tracing ions in the cusp and low-latitude boundary layer using multispacecraft observations and a global MHD simulation, *J. Geophys. Res.*, 107(A9), 1226, doi:10.1029/2001JA000130, 2002.

### 1. Introduction

[2] Statistical analysis of a large data set of particle precipitation observations indicates that the ionospheric foot point of the Earth's magnetospheric cusps extends over only  $\sim 1^\circ$  of latitude and  $\sim 2$  hours local time on either side of noon [Newell and Meng, 1992]. A somewhat broader region of ion and electron precipitation that has fluxes about a factor of 10 lower than the "cusp" is identified as the low-latitude boundary layer (LLBL). This region extends over  $\sim 2^\circ$  of latitude and has a longitude extent of  $\sim 3$  hours on either side of local noon [Newell and Meng, 1992]. When the interplanetary magnetic field (IMF) has a large  $Y$  component, the foot point of the cusp and LLBL can shift significantly in local time such that these regions can be seen at any dayside local time [e.g., Newell *et al.*, 1989].

[3] There is little doubt that ions with magnetosheath energies in the Earth's magnetospheric cusps originate in the

solar wind. Composition measurements in the cusp confirm that these ions cross the magnetopause from the magnetosheath and enter the magnetospheric cusps [e.g., Fuselier *et al.*, 1998]. Recent observations in the cusp also confirm that plasma enters this region through magnetic merging or reconnection. Plasma entry into the cusp by magnetic reconnection can occur when the IMF is northward or southward [see, e.g., Smith and Lockwood, 1996, and references therein]. Both statistical properties of the cusp [e.g., Burch *et al.*, 1985] and individual cusp events [e.g., Onsager *et al.*, 1995] are consistent with plasma entry through reconnection.

[4] The identification of an entry process raises the question of the distinction between the cusp and LLBL as they were originally defined. For southward IMF there is evidence that a large fraction of, if not the entire, dayside magnetopause is open (i.e., reconnection is occurring). Thus the difference between cusp and LLBL or cusp and mantle precipitation has nothing to do with different entry processes. Rather, it is caused by different magnetosheath conditions during plasma entry that give rise to different precipitating energies and fluxes [e.g., Lockwood and Smith, 1993; Newell and Meng, 1993]. Reconnection for northward IMF conditions is somewhat more complicated, but there is also evidence that a good fraction of the dayside magnetopause may be open most of the time [Fuselier *et al.*, 1995].

<sup>1</sup>Lockheed Martin Advanced Technology Center, Palo Alto, California, USA.

<sup>2</sup>Institute of Geophysics and Planetary Physics, University of California, Los Angeles, California, USA.

<sup>3</sup>Los Alamos National Laboratory, Los Alamos, New Mexico, USA.

[5] These interpretations notwithstanding, there is also evidence that part of the LLBL is probably on closed magnetic field lines some of the time. This evidence consists primarily of the observation of trapped or counterstreaming electron distributions on LLBL field lines [e.g., *Oksavik et al.*, 2000]. When the electron population has energies more typical of those found in the magnetosphere (and higher than those found in the magnetosheath), this evidence is most convincing. (While it is relatively easy to create a trapped-like or counterstreaming electron population with magnetosheath energies on open field lines [*Fuselier et al.*, 1995], the higher energy of the magnetospheric electrons makes it difficult to create a similar counterstreaming population on open field lines.) Another convincing piece of evidence is the presence of counterstreaming, low charge state oxygen ( $O^+$ ,  $O^{2+}$ ) on cusp or LLBL field lines [*Dempsey et al.*, 1998; *Fuselier et al.*, 2001]. Low charge state oxygen originates in the ionosphere. Counterstreaming populations indicate that both hemispheres are sources or that there is a single source in one hemisphere and a low-altitude mirror point in the opposite hemisphere. Either interpretation requires closed field lines. While the above evidence of closed field lines containing magnetosheath plasma allows for the possibility of plasma entry processes other than reconnection, it does not eliminate magnetic reconnection. Additional reconnection on a previously opened field line may close the field line.

[6] Thus far, the discussion has been limited to cusp or LLBL ions with energies typical of those found in the magnetosheath (i.e.,  $\sim 1-2$  keV  $e^{-1}$ ). At higher energies there is more controversy over the origin of the ions observed in the cusp and LLBL. In particular, a new population of energetic ions with energies  $>10$  keV  $e^{-1}$  has been observed in the cusp [*Chen et al.*, 1997]. In fact, this population is typically characterized by two separate components, one component with energies up to  $\sim 150$  keV  $e^{-1}$  and a second component with higher energies [*Trattner et al.*, 2001]. Although magnetospheric ions are present at energies  $>10$  keV  $e^{-1}$ , the presence of solar wind ions ( $He^{2+}$ , high charge state oxygen) at energies  $>10$  keV  $e^{-1}$  indicates a solar wind source. Three origins for these ions have been suggested and at least partially investigated.

[7] Recent analysis of the lower-energy component (with energies from  $\sim 10$  up to  $\sim 150$  keV  $e^{-1}$ ) indicates that it probably originates at the Earth's quasi-parallel bow shock. The flux, spectral slope, and composition of the lower-energy component in the cusp and energetic ion population accelerated at the Earth's quasi-parallel bow shock agree to a high degree [*Chang et al.*, 1998; *Trattner et al.*, 2001]. Furthermore, the energetic ion populations in both regions exhibit the same correlation between absolute flux and solar wind density and between spectral slope and solar wind velocity [*Trattner et al.*, 2001]. Thus, from a statistical standpoint, the energetic ion component between  $\sim 10$  and  $150$  keV  $e^{-1}$  in the cusp is the best investigated. These investigations indicate that there is a connection between the quasi-parallel bow shock and the cusp. Although there is evidence of this connection, it has not been demonstrated explicitly by the statistical analysis.

[8] The higher-energy component (above  $150$  keV  $e^{-1}$ ) is not consistent with a bow shock source or any other source

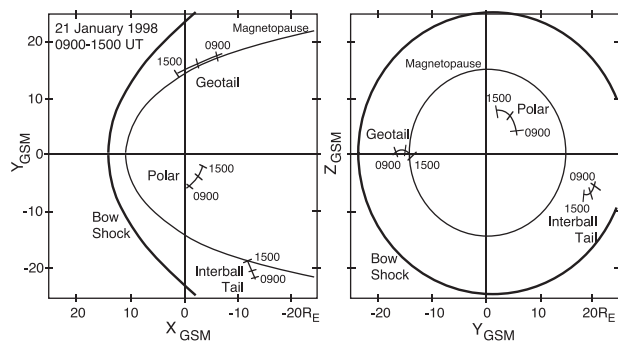


**Figure 1.** Polar, Geotail, and Interball/Tail spacecraft positions on 21 January 1998 from 0900 to 1500 UT. Polar was at high latitudes near the terminator, Geotail was skimming the dawn flank magnetopause near the equatorial plane, and Interball/Tail was on an oblique inbound trajectory toward the duskside magnetopause at southern latitudes.

exterior to the magnetopause. Two possible origins of this population are the duskside magnetosphere and local acceleration in the cusp. Some field lines in the cusp thread the duskside magnetopause. A statistical survey of energetic low charge state oxygen said to be associated with this energetic ion population indicates a bias toward the duskside [*Karra and Fritz*, 1999]. This may support a magnetospheric (and ultimately a plasma sheet) origin of this population. Although the plasma in the plasma sheet is highly processed, composition measurements reveal the presence of  $He^{2+}$  from the solar wind.

[9] Local acceleration of ions in the cusp is the least well investigated. It requires an as yet unidentified acceleration mechanism that resides locally in the cusp. It does not require any direct connection between the cusp and other energetic ion regions such as the duskside magnetosphere or the quasi-parallel shock.

[10] The recent segregation of cusp and LLBL ions into different energies and the apparently conflicting observations of open and closed magnetic field lines in the LLBL have complicated the understanding of the entry and transport of plasma into the Earth's magnetosphere. The purpose of this paper is to present an event observed by multiple spacecraft that has these LLBL characteristics. A global MHD simulation of the event is used to demonstrate how seemingly disparate interpretations of the observations may be combined into a single evolutionary process whereby plasma is transferred into and through the magnetosphere. In section 2 the LLBL observations from the Polar spacecraft are discussed. Section 3 introduces the global MHD simulation and validation data from the Interball/Tail and Geotail spacecraft. Section 4 discusses the results of the application of global MHD to the cusp and LLBL for this event.

## 2. LLBL Observations

[11] Figure 1 shows spacecraft locations on 21 January 1998 from 0900 to 1500 UT. The left panel shows the orbits of Geotail, Polar, and Interball/Tail projected into the  $X$ - $Y$  GSM plane. The right panel shows the three spacecraft

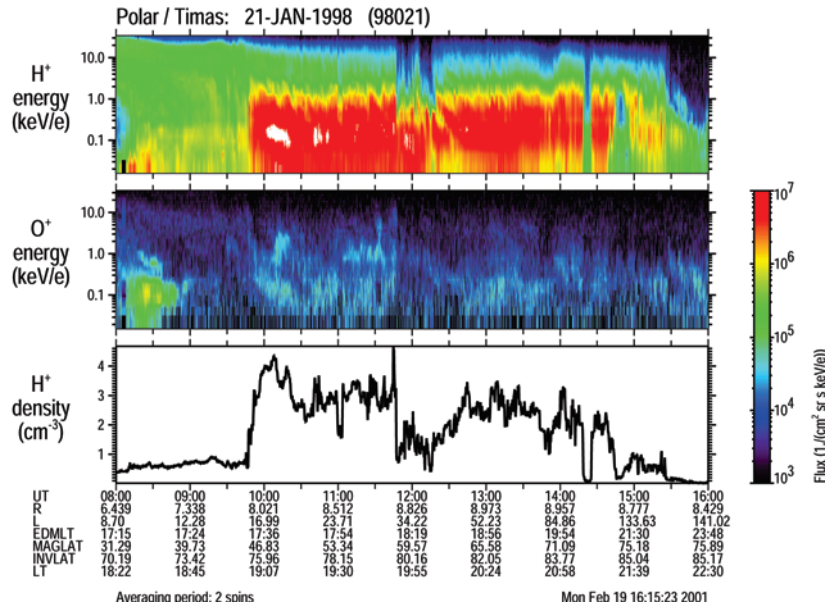


**Figure 2.** (top) Energy-time spectrogram of the omnidirectional  $H^+$  flux, (middle) spectrogram of the omnidirectional  $O^+$  flux, and (bottom) the  $H^+$  density. At 0900 UT the Polar spacecraft was located in the outer magnetosphere at high latitudes. Starting at 0945 UT the  $H^+$  flux below  $\sim 1 \text{ keV } e^{-1}$  was very high, and the density was  $> 1 \text{ cm}^{-3}$ , consistent with low-latitude boundary layer (LLBL) precipitation. The spacecraft remained in this region until the encounter of the lobe at 1420 UT and again at 1530 UT.  $O^+$  is seen throughout the LLBL.

orbits projected onto the  $Y$ - $Z$  GSM plane. At 0900 UT, Polar was on the nightside, near the terminator, and on an outbound trajectory toward apogee. By 1500 UT the spacecraft had passed apogee and was located near the  $Y$ - $Z$  GSM plane  $\sim 2 R_E$  tailward of the terminator. Both Geotail and Interball/Tail were near the magnetopause. Geotail was skimming the dawnside magnetopause in the  $X$ - $Y$  GSM plane starting  $\sim 7 R_E$  tailward of the terminator and ending near the terminator. Interball/Tail was south of the  $X$ - $Y$  GSM plane in the magnetosheath on an oblique inbound trajectory that took it across the magnetopause and into the magnetosphere at 1700 UT.

[12] Although it is not immediately apparent that Polar is in the cusp or LLBL, the spacecraft configuration shown in Figure 1 is excellent for investigating cusp and LLBL properties. In particular, there is more than one spacecraft in the magnetosphere/magnetosheath to provide context measurements, and Polar is in the LLBL measuring plasma that enters the cusp and LLBL. Upstream observations from the Wind spacecraft (located  $\sim 233 R_E$  upstream from the Earth) provide solar wind input to this investigation. The upstream observations on this day are shown in detail in section 3. Briefly, on 21 January 1998 from 0900 to 1500 UT the solar wind velocity was  $\sim 450 \text{ km s}^{-1}$ , the density was  $10$ – $15 \text{ cm}^{-3}$ , and the solar wind dynamic pressure was  $\sim 2.5 \text{ nPa}$ , only slightly higher than a nominal dynamic pressure of  $1.5 \text{ nPa}$ . The magnetic field had a large, positive  $X_{GSE}$  component as well as a large, positive  $Z_{GSE}$  component.

[13] Polar observations from 0800 to 1600 UT from the Toroidal Imaging Mass Angle Spectrograph (TIMAS) [Shelley *et al.*, 1995] are shown in Figure 2. The top panel shows an energy-time spectrogram of the omnidirectional

$H^+$  flux, the middle panel shows a spectrogram of the omnidirectional  $O^+$  flux, and the bottom panel shows the  $H^+$  density derived from the three dimensional  $H^+$  phase space density measured by TIMAS.

[14] At 0900 UT the spacecraft was in the outer magnetosphere at high latitudes. This region was characterized by low  $H^+$  fluxes, densities of  $\sim 0.5 \text{ cm}^{-3}$ , and characteristic energies of several  $\text{keV } e^{-1}$ . Starting at 0945 UT the density increased dramatically, reaching more than  $4 \text{ cm}^{-3}$  by 1000 UT. This density increase was the result of a significant increase in the  $H^+$  flux below  $\sim 2 \text{ keV } e^{-1}$ . The high flux conditions prevailed with some variability until the first encounter with lobe plasma at  $\sim 1420$  UT. By 1530 UT the spacecraft was continuously in the lobe. This region was characterized by low ion fluxes below  $\sim 100 \text{ eV } e^{-1}$  and densities well below  $0.1 \text{ cm}^{-3}$ . (Since the TIMAS instrument has a low-energy cutoff of  $16 \text{ eV } e^{-1}$ , it cannot adequately resolve cold plasma populations that may be present in the lobe.)

[15]  $H^+$  densities from 1000 to 1400 UT were about a factor of 10 below those in the dayside magnetosheath (which would be  $\sim 40 \text{ cm}^{-3}$  for a solar wind density of  $\sim 10 \text{ cm}^{-3}$ ). Thus, despite the fact that the Polar spacecraft was located between 1700 and 2000 magnetic local time (MLT) (Figure 2), the spacecraft was in the region defined previously as the LLBL [Newell and Meng, 1992]. Electron observations from the Polar Hydra instrument [Scudder *et al.*, 1995] (not shown) confirm this region identification. Composition measurements (discussed below) confirm the presence of solar wind plasma below  $\sim 2 \text{ keV } e^{-1}$ . Although solar wind plasma was present during this time period, ionospheric  $O^+$  was present as well. In Figure 2 from 1000 to 1145 UT the  $O^+$  often exhibits peak fluxes at two

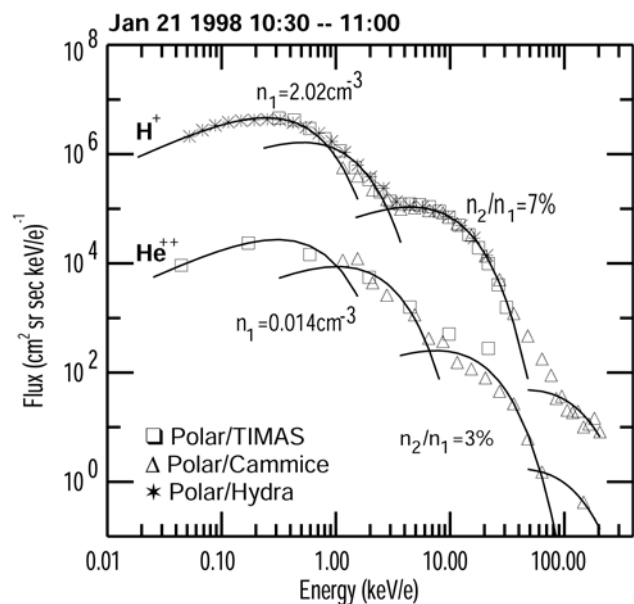


**Figure 3.** Energy spectra for  $H^+$  and  $He^{2+}$  in the cusp/LLBL. Both spectra show several distinct components. The lowest-energy component (below  $3 \text{ keV } e^{-1}$ ) has the bulk of the density. There is a clear break in the energy spectrum at  $\sim 3 \text{ keV } e^{-1}$ , and another break at  $\sim 100 \text{ keV } e^{-1}$ . TIMAS, Toroidal Imaging Mass Angle Spectrograph.

different energies. Some of the  $O^+$  flux at  $\sim 100 \text{ eV } e^{-1}$  in Figure 2 is an instrument artifact. High  $H^+$  fluxes can contaminate the  $O^+$  mass channels in the instrument [Fuselier et al., 2001]. However, mass spectra from the instrument (discussed below) confirm the presence of  $O^+$  at  $\sim 1 \text{ keV } e^{-1}$ .

[16] Figure 3 shows the  $H^+$  and  $He^{2+}$  energy spectra from 1030 to 1100 UT. Data from three ion instruments on the Polar spacecraft (TIMAS, Cammice [Blake et al., 1995], and Hydra [Scudder et al., 1995]) were used to produce these energy spectra. The  $H^+$  and  $He^{2+}$  energy spectra in Figure 3 were fit with Maxwellian distributions to distinguish the components at different energies. Below  $3 \text{ keV } e^{-1}$  the lowest-energy  $H^+$  components (labeled  $n_1$ ) contain the bulk of the plasma density (for details on these low-energy components, see Trattner et al. [2001]). There is a clear break in the  $H^+$  spectrum at  $\sim 3 \text{ keV } e^{-1}$ , with a higher-energy shoulder extending to energies between 50 and  $100 \text{ keV } e^{-1}$ . This component (labeled  $n_2/n_1$  in Figure 3) contains  $\sim 7\%$  of the density of the lowest-energy components. An even higher energy component starts at the break at  $50\text{--}100 \text{ keV } e^{-1}$  and extends to energies  $>200 \text{ keV } e^{-1}$ . Although the statistics are not as good at high energies, the  $He^{2+}$  spectrum exhibits the same components. These energy spectra in Figure 3 are representative of energy spectra from other time periods of high  $H^+$  flux in Figure 2.

[17] Figure 4 shows mass spectra at  $1.72 \text{ keV } e^{-1}$  from TIMAS for the 10-min period starting at 1006 UT. The two spectra are shown for ions propagating parallel (open squares) and antiparallel (solid squares) to the magnetic field. Since the spacecraft was over the Northern Hemisphere, these directions represent toward and away from the northern ionosphere, respectively. The mass spectra show

five distinct peaks, labeled by their respective mass/charge values (obtained from instrument calibration data). The count rates (normalized to the  $H^+$  count rate) toward and away from the ionosphere are well matched, even for ionospheric ions ( $He^+$ ,  $O^{2+}$ , and  $O^+$ ). At this energy the  $He^{2+}$  is a few percent of the  $H^+$  flux, and the  $O^+$  flux is more than 1% of the  $H^+$  flux.  $He^+$  and  $O^{2+}$  fluxes are much lower but still detectable. The mass spectra in Figure 4 are representative of other intervals between 1000 and  $\sim 1145 \text{ UT}$  in Figure 2. After 1145 UT the  $O^+$  fluxes below  $\sim 1 \text{ keV } e^{-1}$  are lower, while the  $He^{2+}$  fluxes are similar to those in Figure 4.

[18] The  $O^+$  fluxes in Figure 4 at  $1.72 \text{ keV } e^{-1}$  are consistent with energized ion outflow from the ionosphere. These energies and fluxes are not consistent with another source of  $O^+$ , namely, the equatorial ring current. The ring current  $O^+$  population peaks at a much higher energy and has a lower flux (compare, for example, the weak  $O^+$  flux at 0800 UT above  $10 \text{ keV } e^{-1}$  in Figure 2 with the more intense flux at 1100 UT at  $\sim 1 \text{ keV } e^{-1}$  in Figure 2). Thus the parallel and antiparallel propagating  $O^+$  must come directly from the northern and southern high-latitude ionospheres, indicating that Polar was on closed field lines.

[19] To summarize, although Polar was located at 1700–2000 magnetic local time, total  $H^+$  fluxes were consistent with LLBL precipitation reported by Newell and Meng [1992]. The  $H^+$  and  $He^{2+}$  energy spectra exhibit several components, including low-energy components below  $3 \text{ keV } e^{-1}$ , a higher-energy component extending to  $\sim 100 \text{ keV } e^{-1}$ , and a very high energy component extending to  $>200 \text{ keV } e^{-1}$ . The energetic ions observed in the LLBL above  $3 \text{ keV } e^{-1}$  were similar to those observed during other cusp intervals [Chang et al., 1998; Trattner et al., 2001].

[20] Mass spectra confirm the presence of magnetosheath ions as well as ionospheric ions. The nearly equal fluxes of ionospheric ions propagating parallel and antiparallel to the

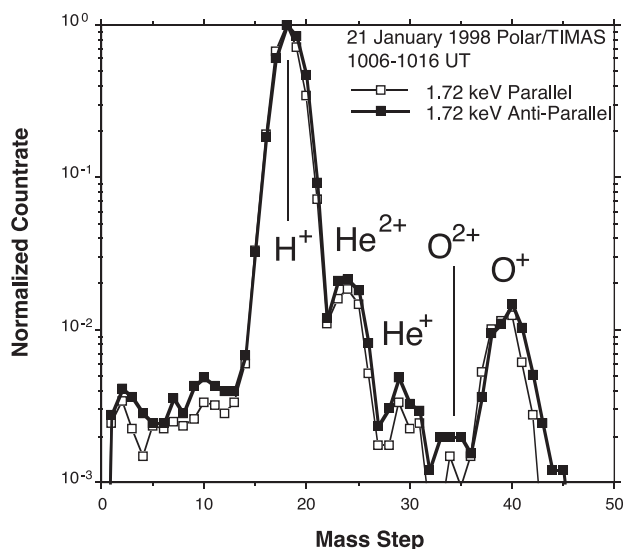


**Figure 4.** Mass spectra from 1006 to 1016 UT at  $1.72 \text{ keV } e^{-1}$ . Solid (open) squares show the normalized count rate antiparallel (parallel) to the magnetic field. Nearly equal fluxes of ionospheric ions  $O^+$ ,  $He^+$ , and  $O^{2+}$  indicate that the spacecraft was on closed magnetic field lines.

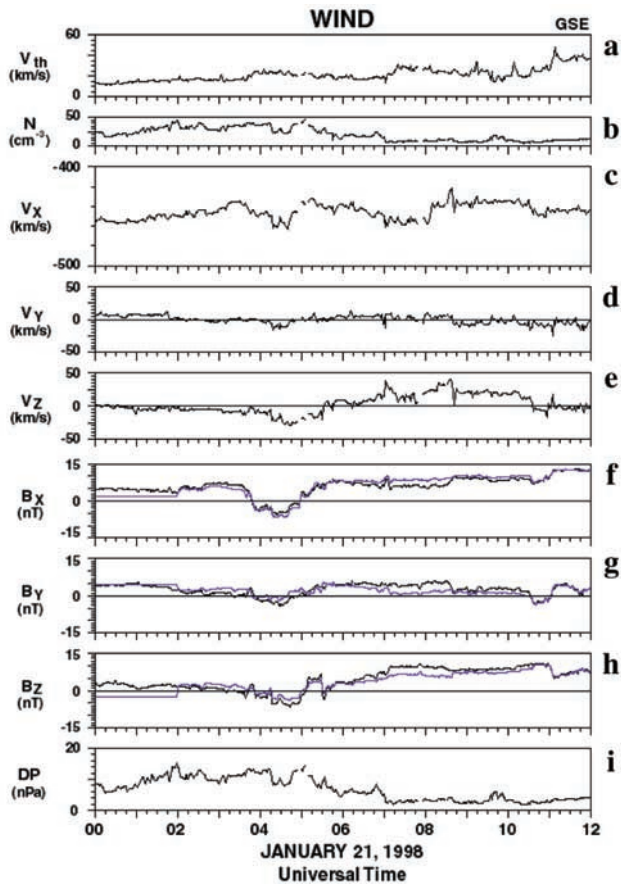


**Figure 5.** Wind spacecraft data used as input to the global MHD simulation: (a) thermal velocity, (b) density, (c–e) three components of the flow velocity, (f–h) three components of the magnetic field, and (i) the dynamic pressure. Black lines show the Wind data, and blue lines show the solar wind used in the simulation.

magnetic field indicate that the //LLBL was on closed magnetic field lines.

### 3. Global MHD Simulation

[21] The magnetospheric part of the global MHD simulation model used in this study is based on a single fluid MHD description. The code solves the normalized resistive MHD equations as an initial value problem, using an explicit conservative predictor-corrector scheme for time stepping and hybridized numerical fluxes for spatial finite differencing [e.g., Berchem *et al.*, 1995a, 1995b, 1998; Raeder *et al.*, 1995, 1996]. A nonlinear function of the local current density is used to model the resistivity term used in Ohm’s law. This model includes a threshold that is a function of the local normalized current density; this threshold is calibrated to avoid spurious dissipation [Raeder *et al.*, 1996]. Similar phenomenological resistivity models have been used in local MHD simulation models [e.g., Sato and Hayashi, 1979] and are based on the assumption that current-driven instabilities are responsible for the anomalous resistivity that produces reconnection at boundaries such as the magnetopause.

[22] The MHD simulation has boundary conditions at low altitudes and in the solar wind upstream from the Earth. At low altitudes a spherical shell with a radius of  $3 R_E$  is placed around the Earth to exclude the region where the Alfvén velocity becomes too large to be computed in the simulation. Inside the shell the MHD equations are not solved, and a static dipole magnetic field is assumed. A two-dimensional ionosphere is assumed to close the field-aligned currents, and the ionospheric potential equation is solved to determine the electrostatic potential self-consistently. A proxy of three ionization sources (solar EUV ionization and discrete and diffuse electron precipitation) is used to compute the ionospheric Hall and Pedersen conductances that are needed to solve the potential equation [Raeder *et al.*, 1996]. The ionospheric potential is then mapped to the shell, where it is used as a boundary condition for the flow velocity.

[23] The solar wind instrument [Ogilvie *et al.*, 1995] and the magnetic field experiment [Lepping *et al.*, 1995] on the Wind spacecraft (located  $233 R_E$  upstream from the Earth) provide the solar wind boundary conditions for the model. Figure 5 shows this solar wind input. In Figures 5a, 5b, 5c, 5d, 5e, 5f, 5g, 5h, and 5i, black lines display the thermal velocity in the solar wind, the density, the three velocity components, the three magnetic field components, and the dynamic pressure, respectively, measured by the Wind spacecraft from 0000 to 1200 UT on 21 January 1998. Both solar wind magnetic field and plasma parameters were advected from the spacecraft location to the inflow boundary of the simulation box located at  $20 R_E$  in front of the Earth before being used as input to the simulation. However, because solar wind measurements are available at only a single location, several assumptions were made. To get input conditions at the simulation boundary, it was assumed that the solar wind plasma convects from the Wind spacecraft location where it is measured to the upstream edge of the simulation box without any dispersion or steepening.

[24] Furthermore, while actual plasma parameters measured by the Wind spacecraft were used, additional processing was required to input the IMF in the simulation. This is because Faraday’s law prevents the advection of the fluctuations of the IMF  $B_x$  component into the simulation system. To alleviate that difficulty, it was assumed that most of the solar wind magnetic field fluctuations lie in parallel planes. This assumption allowed the use of minimum variance analysis over the entire data interval to determine the average normal direction to the magnetic field fluctuations ( $n = 0.463, -0.645, 0.607$ ). Magnetic field data were then rotated from the geocentric solar ecliptic (GSE) system into the new system, which was determined by the normal direction and the two other eigenvectors. Next the magnetic field component along the normal direction was set equal to the magnitude of the average field along that direction. After this transformation the data were rotated back into the simulation’s system of coordinates and propagated to the inflow boundary.

[25] Results of the transformations applied to 1-min-averaged Wind magnetic field data from 0100 to 1200 UT are indicated by the blue lines in Figure 5. They show only small deviations from the actual wind measurements (black lines in Figure 5), indicating that reasonable assumptions were made concerning the structure of the solar wind

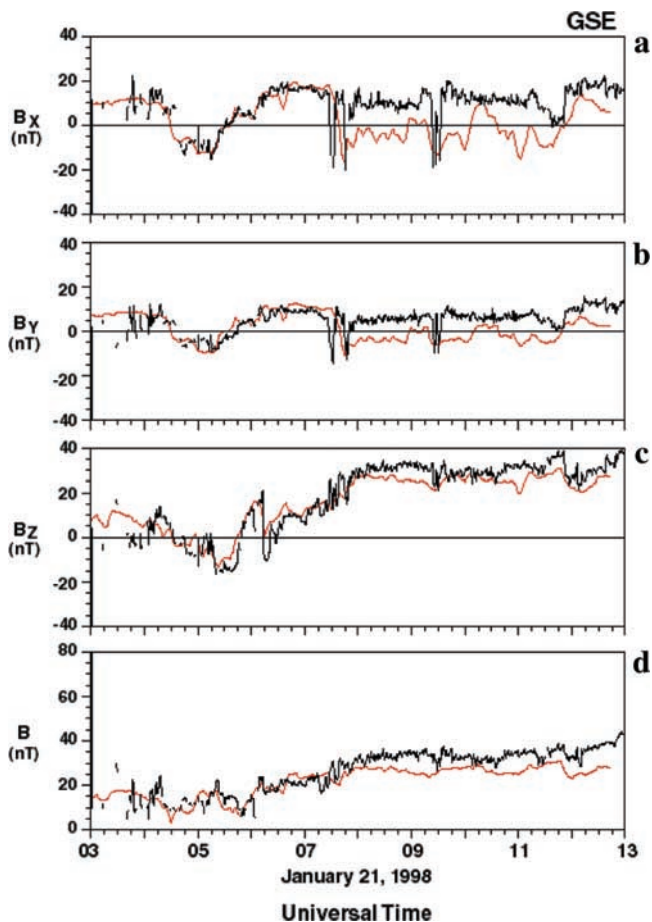


**Figure 6.** Geotail magnetic field data (black lines): (a–d) three components of the magnetic field and the magnitude. The simulation (red lines) reproduces the magnetic field orientation and magnitude well up to 0715 UT. At this time, the spacecraft makes a brief crossing of the magnetopause. After that time, the simulation predicts that the spacecraft remained in the magnetosphere, while the data show that it returned to the magnetosheath except for a brief crossing at  $\sim 0930$  UT.

magnetic field fluctuations during the time interval. The early start time (0100 UT) used to input the solar wind parameters gives the simulation system time to evolve toward a state independent of the initial conditions well before the period of interest. For reference, the transit time of the solar wind through the  $320-R_E$ -long simulation box was about an hour and a half, assuming a constant speed of  $450 \text{ km s}^{-1}$ .

[26] Comparison of the results from this simulation and the Geotail observations in the magnetosheath and magnetosphere is shown in Figure 6. From 0300 to 0730 UT the simulation matches the observations to a high degree. In the simulation and in the observations the Geotail spacecraft is in the magnetosheath near the magnetopause. At  $\sim 0730$  UT the Geotail spacecraft makes a brief excursion into the magnetosphere. The simulation also captures this change of location, but from that time period on, the simulation predicts that the Geotail spacecraft was in the magnetosphere. In fact, Geotail data show that it returned and

remained in the magnetosheath, with the exception of another brief excursion into the magnetosphere at  $\sim 0930$  UT. During this brief excursion the simulation and observations agree. It should not be surprising that the simulation does not reproduce the precise location of magnetospheric boundaries. During this time period the spacecraft was skimming the magnetopause (Figure 1), and a small change ( $<1 R_E$ ) in the magnetopause position is all that is needed to bring the simulations and observations into agreement. The more important result from Figure 6 is that with the exception of this minor disagreement in the spacecraft location, the simulation reproduces the observed global magnetic field configuration in the magnetosheath and dawnside outer magnetosphere.

[27] The MHD simulation also reproduces the magnetic field configuration on the duskside magnetopause. Figure 7 shows the comparison of simulation and Interball/Tail magnetic field data from 0300 to 1300 UT. During this period the spacecraft was in the magnetosheath on an oblique inbound trajectory to the magnetopause (Figure 1), crossing the magnetopause after the period of interest (at  $\sim 1700$  UT). The three components agree well, and the MHD simulation captures both slow and relatively fast rotations in the magnetic field in the magnetosheath.

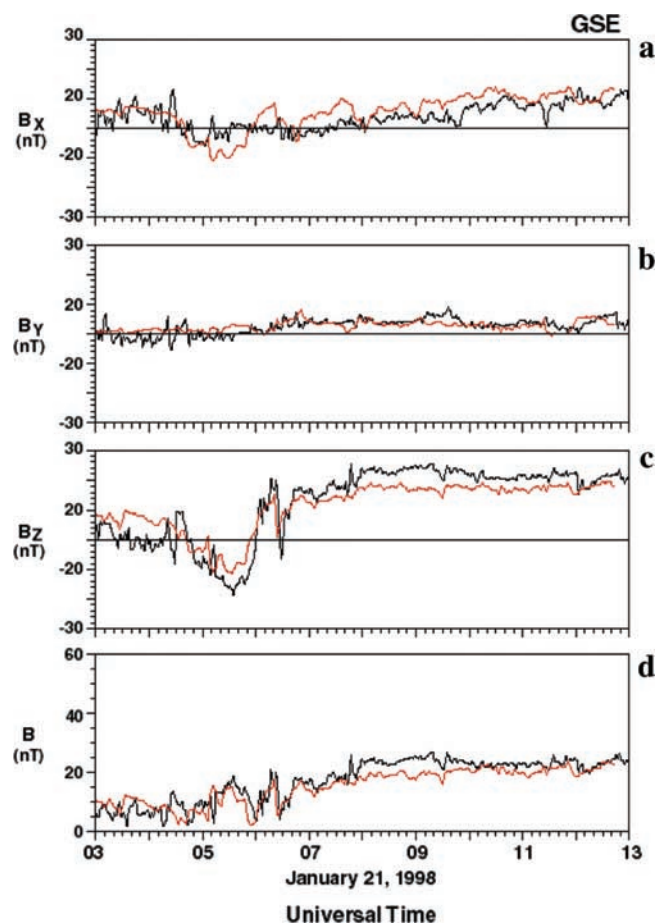


**Figure 7.** Interball/Tail magnetic field data similar to that in Figure 6. The spacecraft remained in the magnetosheath throughout the interval. The simulation predicts the magnetosheath magnetic field orientation very well.

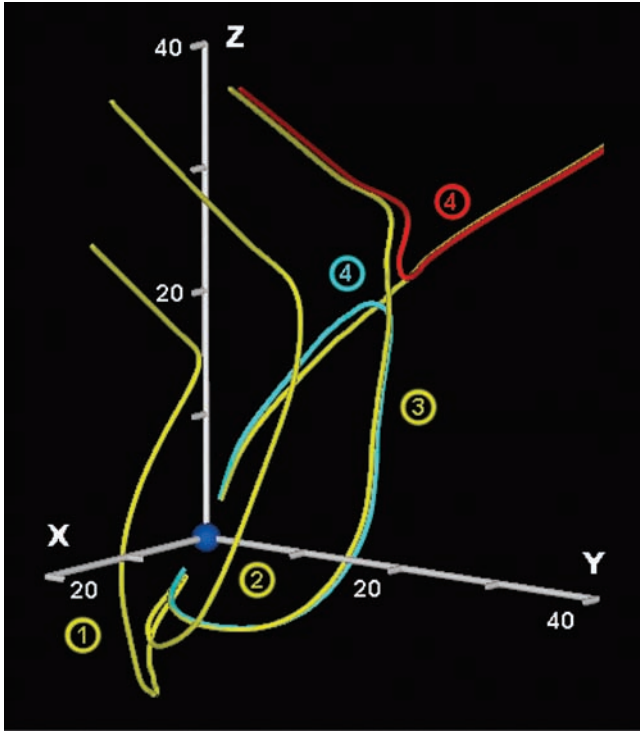


**Figure 8.** Snapshot of selected magnetic field lines from the MHD simulation at 0951 UT. Magnetosheath and magnetospheric field lines first reconnect in the Southern Hemisphere poleward of the cusp (field line 1) because of the dipole tilt and large solar wind  $B_X$  component. These reconnected field lines convect around the duskside magnetopause (field line 2) before reconnecting with a Northern Hemisphere lobe field line (field lines 3 and 4). The second reconnection creates a closed field line containing magnetosheath plasma on the duskside.

[28] The magnetic field configuration on the duskside is particularly important for the Polar observations. Figure 8 shows a snapshot from the MHD simulation (taken at  $\sim 0951$  UT) of selected magnetic field lines on the duskside magnetosphere. The perspective is from 1500 LT and slightly above the equatorial plane. The field lines are numbered in a sequence that would represent a time sequence if the solar wind plasma and magnetic field conditions remained constant. In fact, with the exception of a rotation in the  $Y$  component of the magnetic field at  $\sim 1030$  UT in Figure 5 (when convected to the magnetopause, the effects of this rotation would be observed at  $\sim 1145$  UT), the solar wind conditions remained relatively constant for a long period of time. Therefore, although they represent a snapshot in time, the field lines in Figure 8 can be considered as a temporal sequence of the interaction of a magnetosheath field line with magnetospheric field lines for most of the time period of interest.

[29] Field line 1 (in yellow) is created by reconnection between a draped magnetosheath field line and a lobe field line in the Southern Hemisphere poleward of the southern cusp. The reconnection site is located just tailward of the large kink in the field in the Southern Hemisphere. The reconnection occurs in the Southern Hemisphere first

because the dipole axis is tilted toward the Sun in this hemisphere in January and because of the large positive  $X_{\text{GSM}}$  component to the solar wind magnetic field. The newly reconnected field line starts in the ionosphere on the dawnside and drapes against the magnetopause, eventually exiting the bow shock on the duskside. Because of the view perspective, the field line appears to extend in the  $-Y$  direction outside the bow shock. In reality, the IMF has a  $+Y$  component. Field line 2 (also in yellow) shows the reconnected field line at a later time when it has convected to the duskside magnetopause. This convection is the result of the positive  $B_Y$  component in the solar wind, which causes the draped field line to be dragged duskward. Field line 3 (also in yellow) shows this still open field line at an even later time, just before it reconnects a second time in the high-latitude Northern Hemisphere. By this time, the field line is mostly in the magnetosphere and exits the magnetopause tailward of the dusk terminator. The second reconnection creates field line 4. The red field line 4 has both ends in interplanetary space and is the result of the reconnection of the high-latitude part of field line 3 with the tailward part of a Northern Hemisphere lobe field line (that is also open). The Polar spacecraft is located on the other field line 4 in blue. This closed field line is created by the reconnection of the magnetospheric part of field line 3 with the magnetospheric part of the Northern Hemisphere lobe field line.

[30] The field line evolution shown in Figure 8 persists throughout most of the interval in Figure 2 because the solar wind magnetic field is persistently northward and has a persistent, large  $B_X$  component and positive  $B_Y$  component (Figure 5). There is one period when this evolution is interrupted. In Figure 5, from  $\sim 1030$  to 1100 UT, the  $B_Y$  component of the solar wind magnetic field changes orientation from duskward (positive  $B_Y$ ) to dawnward (negative  $B_Y$ ) and then back to duskward. The effect of this rotation (when convected from the upstream monitor to the Earth's magnetosphere) can be seen in the spectrogram in Figure 2 from  $\sim 1145$  to 1215 UT. The flux of energetic  $\text{H}^+$  above  $5 \text{ keV } e^{-1}$  and the total density decrease dramatically. The reason for this change in the energetic  $\text{H}^+$  flux and the density is probably related to the change in the draped magnetosheath magnetic field from a duskward to a dawnward orientation. After the solar wind magnetic field resumes its original duskward orientation, the Polar spacecraft once again observes a  $\text{H}^+$  population similar to the one before 1145 UT and the evolution shown in Figure 8 resumes. This continues until the spacecraft moves onto lobe field lines at  $\sim 1500$  UT.

#### 4. Discussion

[31] The plasma populations observed on closed magnetic field lines in the LLBL by Polar are the result of mixing from all sources that had access to those magnetic field lines over their history. The MHD simulation results (Figure 8) offer the interpretation that the closed LLBL field line observed by Polar (field line 4 in blue) was created by multiple reconnections. Thus the low-energy plasma component, below  $3 \text{ keV } e^{-1}$  in Figures 2 and 3, accessed the magnetosphere through reconnection of a draped magnetosheath field line with a lobe field line. The reconnection

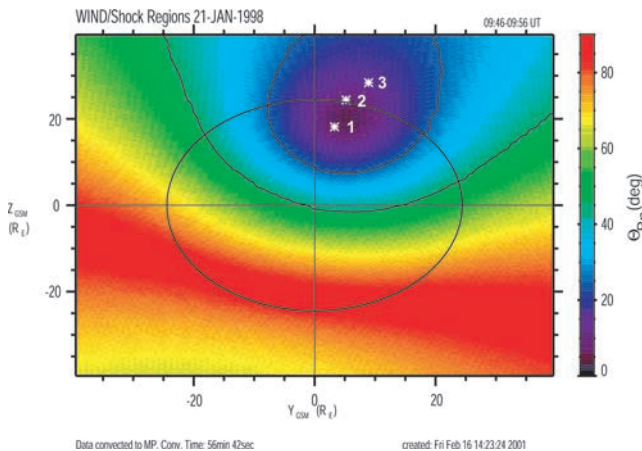


**Figure 9.**  $\theta_{Bn}$  as a function of position on the bow shock. The view is from the Sun, the solid oval is the location of the terminator, the dashed line in the green region is the boundary between quasi-perpendicular ( $\theta_{Bn} > 45^\circ$ ) and quasi-parallel ( $\theta_{Bn} < 45^\circ$ ), and the dashed line at the boundary between the blue and violet regions identifies  $\theta_{Bn} = 25^\circ$ . The shock conditions in the subsolar region were only nominally quasi-parallel; however, at high northern latitudes the shock conditions were nearly parallel. The asterisks labeled 1, 2, and 3 depict the location where the reconnected field lines 1, 2, and 3 in Figure 8 exit the bow shock.

occurred first in the Southern Hemisphere, forming the southern high-latitude cusp precipitation and leaving the field line open to interplanetary space in the high-latitude Northern Hemisphere. The second reconnection in the Northern Hemisphere created a closed field line identified in the Polar data as the LLBL. While the field lines were open, ionospheric ions flowed continuously out of the Northern and Southern Hemispheres. Thus, on the closed field line, Polar observed these two ionospheric sources as equal fluxes of ionospheric oxygen and helium propagating parallel and antiparallel to the closed magnetic field line (Figure 4).

[32] Figure 9 shows that the higher-energy component (between 3 and 100 keV  $e^{-1}$  in Figure 3) observed by Polar on the closed LLBL field lines probably originated at the quasi-parallel bow shock. The angle between the shock normal and the solar wind magnetic field ( $\theta_{Bn}$ ) is color-coded with red ( $>70^\circ$ ) and violet ( $<20^\circ$ ). The view is from the Sun, the solid oval is the intersection of the bow shock with the terminator ( $X = 0$ ), the dashed line in the green region is the boundary between the quasi-perpendicular ( $\theta_{Bn} > 45^\circ$ ) and quasi-parallel ( $\theta_{Bn} < 45^\circ$ ) shock, and the dashed line at the boundary between the blue and violet regions identifies  $\theta_{Bn} = 25^\circ$ . The shock conditions in the subsolar region were only nominally quasi-parallel; however, at high northern latitudes the shock conditions were nearly parallel. The asterisks labeled 1, 2, and 3 indicate the location where the reconnected field lines 1, 2, and 3 in Figure 8 exit the bow shock. It is clearly evident that prior to the second reconnection that closed the field line in the magnetosphere, the open magnetic field line in the southern cusp had direct connection to the quasi-parallel bow shock.

Therefore energetic ions accelerated at the quasi-parallel bow shock had direct access to the magnetosphere through the cusp. When the second reconnection occurred that created the LLBL on closed field lines, these shock-accelerated ions were trapped, creating the energetic ion component between 3 and 100 keV  $e^{-1}$  observed by Polar (Figure 2).

[33] The highest-energy component ( $>100$  keV  $e^{-1}$ ) observed by Polar in the LLBL could have two possible origins. One origin is the duskside magnetopause, and the other is local acceleration in the cusp.

[34] The closed magnetic field line observed by Polar was created by reconnection in the Southern Hemisphere and convection of the reconnected field line along the entire dusk flank magnetopause. While the field line is convecting, energetic magnetospheric ions drifting from the nightside could access this open field line. Confirmation of this process requires test particle tracing in the MHD simulation (which is beyond the scope of this paper) or separate observations of an energetic ion component in the magnetosphere near the magnetopause (no spacecraft were in position to observe this component directly). However, there is no reason to expect that particle tracings would produce something different from previous studies. It is well known that energetic magnetospheric ion drift paths intersect the dayside and flank magnetopause on the duskside [Takahashi and Iyemori, 1989]. Therefore they have access to the field line that ultimately becomes the closed LLBL field line 4 in blue in Figure 8.

[35] In summary, a single evolutionary process can explain observations in the LLBL on 21 January 1998. The distinct ion populations observed on closed field lines in the LLBL are the result of accumulation from different sources as reconnected lobe-magnetosheath field lines in the cusp convect around the duskside, undergo a second reconnection, and close to form the LLBL. Sources with direct access to the ultimately closed LLBL field lines observed by Polar are the dayside magnetosheath (low-energy ions below 3 keV  $e^{-1}$ ), the quasi-parallel bow shock (higher-energy ions between 3 and 100 keV  $e^{-1}$ ), and possibly the duskside magnetopause (highest-energy ions above 100 keV  $e^{-1}$ ).

[36] **Acknowledgments.** Research at Lockheed Martin was conducted under the NASA Guest Investigator Program through a subcontract from Southwest Research Institute (contract 999095Q) and through ISTP grant NAG5-8072 and contract NASS-30302. Research at UCLA was supported by NASA grants NAS5-9071 and NAS5-6689. Solar wind data from Wind were provided by K. Ogilvie and R. Lepping through the CDAWeb. Geotail and Interball/Tail data were also provided through the CDAWeb. This paper is the result of a collaboration developed during several workshops on multispacecraft observations that were held at the International Space Science Institute in Bern, Switzerland. The authors gratefully acknowledge A. Pedersen for leading the workshops and the ISSI for their support.

[37] Janet G. Luhmann thanks Daniel M. Ober and Dag A. Lorentzen for their assistance in evaluating this paper.

## References

- Berchem, J., J. Raeder, and M. Ashour-Abdalla, Reconnection at the magnetospheric boundary: Results from global magnetohydrodynamic boundary, in *Physics of the Magnetopause*, *Geophys. Monogr. Ser.*, vol. 90, edited by B. U. Ö. Sonnerup, P. Song, and M. F. Thomsen, p. 205, AGU, Washington, D.C., 1995a.
- Berchem, J., J. Raeder, and M. Ashour-Abdalla, Flux ropes at the magnetospheric boundary, *Geophys. Res. Lett.*, 22, 1189, 1995b.

- Berchem, J., J. Raeder, M. Ashour-Abdalla, L. A. Frank, W. R. Paterson, K. L. Ackerson, S. Kokubun, T. Yamamoto, and R. P. Lepping, The distant tail at 200 *Re*: Comparison between Geotail observations and the results of a global simulation, *J. Geophys. Res.*, *103*, 9121, 1998.
- Blake, J. B., et al., CEPPAD, in *The Global Geospace Mission*, edited by C. T. Russell, p. 531, Kluwer Acad., Norwell, Mass., 1995.
- Burch, J. L., P. H. Reiff, J. D. Menietti, R. A. Heelis, W. B. Hanson, S. D. Shawhan, E. G. Shelley, M. Suguira, D. R. Weimer, and J. D. Winningham, IMF By-dependent plasma flow and Birkeland currents in the dayside magnetosphere, 1, Dynamics Explorer observations, *J. Geophys. Res.*, *90*, 1577, 1985.
- Chang, S.-W., et al., Cusp energetic ions: A bow shock source, *Geophys. Res. Lett.*, *25*, 3729, 1998.
- Chen, J., T. A. Fritz, R. B. Sheldon, H. E. Spence, W. N. Spjeldvik, J. F. Fennell, and S. Livi, A new, temporarily confined population in the polar cap during the August 27, 1996 geomagnetic field distortion period, *Geophys. Res. Lett.*, *24*, 1447, 1997.
- Dempsey, D. L., J. L. Burch, M. M. Huddleston, C. J. Pollock, J. H. Waite Jr., M. Wüest, T. E. Moore, and E. G. Shelley, Reflected solar wind ions and downward accelerated ionospheric ions during the January 1997 magnetic cloud event, *Geophys. Res. Lett.*, *25*, 2979, 1998.
- Fuselier, S. A., B. J. Anderson, and T. G. Onsager, Particle signatures of magnetic topology at the magnetopause: AMPTE/CCE observations, *J. Geophys. Res.*, *100*, 11805, 1995.
- Fuselier, S. A., E. G. Shelley, W. K. Peterson, and O. W. Lennartsson, Solar wind He<sup>2+</sup> and H<sup>+</sup> distributions in the cusp for southward IMF, in *Polar Cap Boundary Phenomena*, edited by J. Moen, A. Egeland, and M. Lockwood, *NATO ASI Ser., Ser. C*, *509*, 63, 1998.
- Fuselier, S. A., S. M. Petrinc, K. J. Trattner, and W. K. Peterson, O<sup>+</sup> observations in the cusp: Implications for dayside magnetic field topology, *J. Geophys. Res.*, *106*, 5977, 2001.
- Karra, M., and T. A. Fritz, Energy dispersion features in the vicinity of the cusp, *Geophys. Res. Lett.*, *26*, 3553, 1999.
- Lepping, R. P., et al., The wind magnetic field investigation, in *The Global Geospace Mission*, edited by C. T. Russell, p. 207, Kluwer Acad., Norwell, Mass., 1995.
- Lockwood, M., and M. F. Smith, Comment on "Mapping the dayside ionosphere to the magnetosphere according to particle precipitation characteristics" by Newell and Meng, *Geophys. Res. Lett.*, *20*, 1739, 1993.
- Newell, P. T., and C.-I. Meng, Mapping the dayside ionosphere to the magnetosphere according to particle precipitation characteristics, *Geophys. Res. Lett.*, *19*, 609, 1992.
- Newell, P.T., and C.-I. Meng, Reply, *Geophys. Res. Lett.*, *20*, 1741, 1993.
- Newell, P. T., C.-I. Meng, D. G. Sibeck, and R. Lepping, Some low-altitude cusp dependencies on the interplanetary magnetic field, *J. Geophys. Res.*, *94*, 8921, 1989.
- Ogilvie, K. W., et al., A comprehensive plasma instrument for the Wind spacecraft, in *The Global Geospace Mission*, edited by C. T. Russell, p. 55, Kluwer Acad., Norwell, Mass., 1995.
- Oksavik, K., F. Søråas, J. Moen, and W. J. Burke, Optical and particle signatures of magnetospheric boundary layers near magnetic noon: Satellite and ground-based observations, *J. Geophys. Res.*, *105*, 27555, 2000.
- Onsager, T. G., S.-W. Chang, J. D. Perez, J. B. Austin, and L. X. Janoo, Low-altitude observations and modeling of quasi-steady magnetopause reconnection, *J. Geophys. Res.*, *100*, 11831, 1995.
- Raeder, J., R. J. Walker, and M. Ashour-Abdalla, The structure of the distant geomagnetic tail during long periods of northward IMF, *Geophys. Res. Lett.*, *22*, 349, 1995.
- Raeder, J., J. Berchem, and M. Ashour-Abdalla, The importance of small scale processes in global MHD simulations: Some numerical experiments, in *Physics of Space Plasmas*, edited by T. Chang and J. R. Jasperse, p. 403, Mass. Inst. of Technol., Cambridge, 1996.
- Sato, T., and T. Hayashi, Externally driven magnetic reconnection and a powerful magnetic energy converter, *Phys. Fluids*, *22*, 1189, 1979.
- Scudder, J. D., et al., Hydra: A 3-dimensional electron and ion hot plasma instrument for the polar spacecraft of the GGS mission, in *The Global Geospace Mission*, edited by C. T. Russell, p. 459, Kluwer Acad., Norwell, Mass., 1995.
- Shelley, E. G., et al., The toroidal imaging mass-angle spectrograph (TIMAS) for the Polar mission, in *The Global Geospace Mission*, edited by C. T. Russell, p. 497, Kluwer Acad., Norwell, Mass., 1995.
- Smith, M. F., and M. Lockwood, Earth's magnetospheric cusps, *Rev. Geophys.*, *34*, 233, 1996.
- Takahashi, S., and T. Iyemori, Three-dimensional tracings of charged particle trajectories in a realistic magnetospheric model, *J. Geophys. Res.*, *94*, 5505, 1989.
- Trattner, K. J., S. A. Fuselier, W. K. Peterson, S.-W. Chang, R. Friedel, and M. R. Aellig, Origins of energetic ions in the cusp, *J. Geophys. Res.*, *106*, 5967, 2001.

---

S. A. Fuselier and K. J. Trattner, Lockheed Martin Advanced Technology Center, Palo Alto, CA 94304-1191, USA. (fuselier@spasci.com)  
 J. Berchem, Institute of Geophysics and Planetary Physics, University of California, Los Angeles, CA 90095-1567, USA. (jberchem@igpp.ucla.edu)  
 R. Friedel, Los Alamos National Laboratory, Los Alamos, NM 87545, USA. (friedel@nis.lanl.gov)